Assembling of gold nanorods on P(NIPAM-AAPBA) microgels: A large shift in the plasmon band and colorimetric glucose sensing

ARTICLE *in* RSC ADVANCES · JUNE 2012

Impact Factor: 3.84 · DOI: 10.1039/c2ra20466e

4 AUTHORS, INCLUDING:

Yongjun Zhang
Nankai University
89 PUBLICATIONS **1,780** CITATIONS

SEE PROFILE

RSC Advances

Dynamic Article Links

Cite this: *RSC Advances*, 2012, **2**, 4768–4776

www.rsc.org/advances

PAPER

Assembling of gold nanorods on P(NIPAM–AAPBA) microgels: a large shift in the plasmon band and colorimetric glucose sensing†

Yapeng Zhang, Kun Liu, Ying Guan and Yongjun Zhang*

Received 13th March 2012, Accepted 14th March 2012
DOI: 10.1039/c2ra20466e

Amine modified gold nanorods (GNR) were assembled onto the surface of poly(*N*-isopropylacrylamide-*co*-3-acrylamidophenylboronic acid) (P(NIPAM–AAPBA)) microgel particles *via* electrostatic interactions. The effects of pH and GNR/microgel ratio on the self-assembly were studied. It was revealed that GNRs can be sequestered more effectively at a higher pH because the surface charge density of the microgel particles increases with increasing pH. In addition, the surface coverage of the GNRs increases with increasing GNR/microgel ratio. Based on these observations hybrid microgels were prepared at pH 8.5 and 9.0 using a high GNR/microgel ratio. Upon heating these hybrid microgels exhibit a redshift of over 100 nm in their plasmon band, which is much larger than those reported in the literature. At the same time, the color of the microgel dispersion gradually changes from blue to grey. The hybrid microgel can be regarded to have a core/shell-like structure, as the radius increase of the hybrid microgel, either at a fully swollen state or a fully collapsed state, is comparable to the diameter of the GNRs. The thermal phase transition of the hybrid microgel starts at the same temperature as that of the bare microgel, but ends at a much higher temperature. The widened phase transition is attributed to the restriction of the non-thermosensitive GNR shell on the deswelling of the core. Similarly glucose-induced swelling is also retarded, resulting in a reduced glucose-sensitivity. The glucose-induced swelling also results in the blueshift of the plasmon band and color change of the sample. The new hybrid microgel can be used as a dual colorimetric sensor for temperature and glucose.

Introduction

Microgels are spherical hydrogel particles with diameters ranging from tens of nanometers to several microns.[1] Among the various microgels, the poly(*N*-isopropylacrylamide) (PNIPAM) microgel, which can undergo a temperature-triggered, reversible volume phase transition, may be the most widely studied.[2] A lot of PNIPAM-based microgels with novel structures and functionalities have been synthesized. These smart materials have found numerous applications in biomedical areas,[3,4] such as in drug delivery,[5,6] biosensing,[7–9] and for use as cell scaffolds.[10,11] For the functionalization of PNIPAM microgels, a commonly used method is the introduction of a suitable functional group. Using this strategy, PNIPAM microgels sensitive to stimuli other than temperature, such as pH,[12,13] light,[14] glucose,[15–18] Pb^{2+}[19] and K^{+}[20] have been synthesized. Another strategy is to introduce inorganic nanoparticles.[21] In this way, novel hybrid microgels with unique optical,[22–24] magnetic[25,26] or catalytic properties[27,28] were synthesized.

Noble metal nanoparticles, such as gold nanoparticles (GNPs), exhibit surface plasmon resonance bands in the visible region with absorption coefficients several orders of magnitude higher than those of common organic dyes.[29] The position of the plasmon bands strongly depends on the size and shape of the particles. More importantly they are highly sensitive to the dielectric nature of the surrounding environment. Therefore these materials have great potential to be used as optical transducers in biosensors.[30–32] Two sensing modes have been developed to design GNP-based colorimetric sensors. The first exploits the sensitivity of the plasmon bands to the local refractive index of the surrounding medium to report the binding of a biomolecule,[33] while the second exploits the sensitivity of the plasmon bands to the proximity of nanoparticles.[34,35] In the second mode, the addition of an analyte induces the aggregation of nanoparticles. As the particles approach each other, the plasmon band shifts to longer wavelength due to the long-range coupling of surface plasmons. Compared with the first mode, the aggregation-induced optical signals are usually much more pronounced.

Novel GNP/PNIPAM hybrid microgels have been synthesized by the assembly of GNPs on the surface of PNIPAM microgel

Key Laboratory of Functional Polymer Materials and State Key Laboratory of Medicinal Chemical Biology, Institute of Polymer Chemistry, College of Chemistry, Nankai University, Tianjin, 300071, China. E-mail: yongjunzhang@nankai.edu.cn; Tel: 86-22-23501657

† Electronic Supplementary Information (ESI) available: TEM image of gold nanorods, FTIR and UV-vis spectra of the as-prepared and amine modified gold nanorods. See DOI: 10.1039/c2ra20466e/

particles,[22,36–38] or the *in situ* growth of GNP on the surface or in the interior of microgel particles,[23,39] or polymerization of NIPAM using GNPs as the core.[40–42] On one hand, loading of GNPs on microgel particles will improve their storage stability and allow for their repeated application. On the other hand, stimuli-triggered (de)swelling of the microgel particles can be facilely determined through the shift of the plasmon band of the GNPs. Therefore these novel hybrid microgels, combining the strengths of both components, have great potential in many applications including biosensing. However, up to now this system has only been used to detect physical changes such as temperature,[22] pH[36] and ionic strength.[43] In addition, the band shift achieved up to now has been relatively small. In this contribution, gold nanorods (GNRs) were assembled onto glucose-sensitive poly(*N*-isopropylacrylamide-*co*-3-acrylamidophenylboronic acid) (P(NIPAM–AAPBA)) microgels. We observed a temperature-induced plasmon band shift of over 100 nm which is the largest reported to the best of our knowledge. We also showed that this system can be developed as novel colorimetric glucose sensor.

Experimental section

Materials

N-Isopropylacrylamide (NIPAM) was purchased from Tokyo Chemical Industry Co., Ltd. *N*,*N*′-Methylenebis (acrylamide) (BIS) and 3-aminophenylboronic acid (APBA) were purchased from Alfa Asear. Acrylic acid (AA) was purchased from ACROS. Sodium dodecyl sulfate (SDS) and cystamine dihydrochloride were purchased from Sigma-Aldrich. *N*-(3-Dimethylaminopropyl)-*N*′-ethylcarbodiimide hydrochloride (EDC), potassium persulfate (KPS), cetyltriethylammonium bromide (CTAB), $HAuCl_4$, $AgNO_3$ and ascorbic acid were purchased from local providers. NIPAM was purified by recrystallization from a hexane/acetone mixture and dried in a vacuum. AA was distilled under reduced pressure. Other reagents were used as received.

Synthesis of the P(NIPAM–AAPBA) microgel

The poly(*N*-isopropylacrylamide-*co*-acrylic acid) (P(NIPAM–AA)) microgel was synthesized as follows. 1.400 g of NIPAM, 0.100 g of AA, 0.033 g of BIS and 0.039 g of SDS were dissolved in 100 mL of water. The reaction mixture was filtered and transferred to a three-necked round-bottom flask equipped with a condenser and a nitrogen line. It was purged with nitrogen for 30 min and then heated to 70 °C. 5 mL of 0.06 M KPS solution was added to initiate the reaction and the reaction was allowed to proceed for 4 h. The resultant microgels were purified by dialysis (cutoff 12 000–14 000) against water with at least twice daily water changes for 2 weeks.

The P(NIPAM–AAPBA) microgel was then prepared by modifying the P(NIPAM–AA) microgel with APBA as follows. 0.233 g of APBA was dissolved in 45 mL of water and added to 5 mL of the purified P(NIPAM–AA) microgel. The mixture was cooled to ~4 °C with an ice bath, to which 0.239 g of EDC was added. The reaction mixture was kept at about 4 °C for 4 h. The resultant products were purified by dialysis against water.

Synthesis of GNRs

GNRs were synthesized according to ref. 44. Briefly, a 10 mL reaction mixture was first prepared with the final concentrations of CTAB, $HAuCl_4$, $AgNO_3$ and ascorbic acid were 0.1 M, 1 mM, 0.2 mM and 2 mM, respectively. Then 50 μL of cold $NaBH_4$ (final concentration = 1 mM) was rapidly added under stirring. The reaction was allowed to proceed at room temperature for 6 h.

Amine modification of GNRs

10 mL of the as-prepared GNRs was centrifugated at 8000 rpm for 30 min. The supernatant was discarded and the particles were redispersed in 10 mL of deionized water. After adding 1 mL of 30 mM cystamine dihydrochloride, the solution was sonicated at 50 °C for 3 h. Finally excess CTAB and cystamine dihydrochloride were removed in the supernatant fraction by centrifugation at 8000 rpm for 10 min and the particles were redispersed in deionized water.[45]

Assembly of GNRs on microgel particles

Different amounts of P(NIPAM–AAPBA) microgel was first diluted with 5 mL of 20 mM phosphate buffer. After being cooled in an ice bath, different amounts of GNRs were injected rapidly. The resulting mixture was stirred for 1 more hour in the ice bath. Detailed amounts of microgel and GNR are listed in Table 1.

Characterizations

The size of the microgel particles were measured by dynamic light scattering with a Brookhaven 90Plus laser particle size analyzer. All the measurements were carried out at a scattering angle of 90°. The sample temperature was controlled with a built-in Peltier temperature controller. UV-vis spectra were measured on a TU-1810PC UV-Vis spectrophotometer (Purkinje General, China)

Table 1 Assembly of GNRs onto P(NIPAM–AAPBA) microgel spheres[a]

Entry	pH	GNR/Microgel ratio[b]	Microgel	GNR	T-induced plasmon shift
1	7.0	1	200 μL	600 μL (0.5 mM)	8 nm
2	8.0	1	200 μL	600 μL (0.5 mM)	13 nm
3	8.5	1	200 μL	600 μL (0.5 mM)	17 nm
4	9.0	1	200 μL	600 μL (0.5 mM)	19 nm
5	8.5	2.88	200 μL	160 μL (5.4 mM)	34 nm
6	8.5	21.6	50 μL	300 μL (5.4 mM)	106 nm
7	9.0	21.6	20 μL	125 μL (5.4 mM)	175 nm

[a] Assembly was carried out by sequentially adding various amounts of (PNIPAM–AAPBA) microgels and GNRs to 5 mL of phosphate buffer at ~5 °C. [b] The ratio was expressed as times that in Entry 3.

using water as the reference. The sample temperature was controlled with a refrigerated circulator. TEM images were acquired with a Philips T20ST transmission electron microscope. The zeta potential of the P(NIPAM–AAPBA) microgel was measured on a Brookhaven ZetaPlus Zeta Potential Analyzer at 10 °C. The samples were highly dilute microgel dispersions prepared using phosphate buffers of various pHs.

Results and discussion

Assembling of GNRs on P(NIPAM-AAPBA) microgel particles

In this work we adopted E. Kumacheva *et al.*'s[37,38,46] and M. Karg *et al.*'s [22,36] method to assemble GNRs onto the surface of P(NIPAM–AAPBA) microgel particles. As mentioned above, hybrid microgels have also been synthesized by the *in situ* growth of GNPs on the surface or in the interior of microgel particles,[23,39] or polymerization of NIPAM using GNPs as the core.[40–42] Compared with these methods, the self-assembly method allows for fine control of the structure and properties of the two components, since they are prepared separately in advance. Here we synthesized the P(NIPAM–AAPBA) microgel by the modification of the (P(NIPAM–AA) microgel with 3-aminophenylboronic acid under EDC catalysis as reported previously (Scheme 1).[16] The thermosensitivity and glucose-sensitivity of this microgel have been thoroughly characterized. GNRs, which are ~30 nm in length and ~13 nm in diameter, were synthesized according to ref. 44 (Fig. 1S†).

The driving force for the assembly is the electrostatic interaction between the positively charged nanorods and the negatively charged microgel particles.[22,36,46] Although the as-prepared GNRs bear some positive charges, they were previously coated with a polyelectrolyte bilayer (poly(styrene sulfonate)/poly(diallyldimethylammonium chloride)) to enhance colloidal stability and to achieve a positively charged surface.[22,36,38] For the same reason, here the nanorods were modified with cystamine dihydrochloride to introduce amino groups on the surface, using a method developed by Wang and Irudayaraj.[45] The successful introduction of amino groups was confirmed by the appearance of the N–H stretching band in the IR spectrum of the nanorods (Fig. 2S†). Compared with that of the as-prepared nanorods, the longitudinal plasmon band of the modified nanorods shifts from 628 nm to 636 nm (Fig. 3S†), indicating

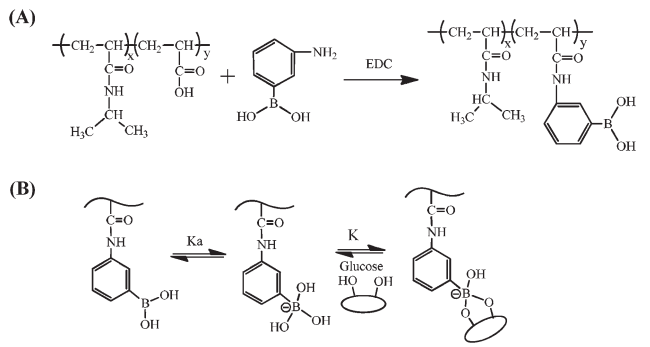

Scheme 1 (A) Synthesis of P(NIPAM–AAPBA) microgels by modification of P(NIPAM–AA) microgels with 3-aminophenyboronic acid, and (B) the complexation equilibrium between the phenylboronic acid derivative and glucose.

an increase in the local refractive index of the surrounding medium. No aggregation of the GNRs was observed during the modification as reported by Wang and Irudayaraj.[45]

The amine modified nanorods were then mixed with the P(NIPAM–AAPBA) microgel to prepare the hybrid microgel. We first examined the effects of two major factors, *i.e.*, pH and the ratio of nanorod to microgel, on the self-assembly of the nanorods. The first series of experiments were conducted to study the effect of pH (Entries 1–4, Table 1). To this end, the P(NIPAM–AAPBA) microgel was dispersed in 20 mM phosphate buffer of various pHs. To obtain a large surface area for GNR deposition, the microgel dispersions were first cooled to ~5 °C with an ice bath and then the GNRs were added. The ratio of GNR to P(NIPAM–AAPBA) microgel is the same for all samples in this series. Then the evolution of the UV/Vis spectra during a heating process was followed. As shown in Fig. 1, a red-shift of the longitudinal plasmon band was observed for all samples, while the shift of the transverse band is negligible. The redshift of the plasmon band can be explained by the shrinking of the microgel particles during the heating process, as already revealed by other authors.[22] Although the trend is similar for all samples, close examination reveals some differences. One difference is that the intensity of the longitudinal plasmon band does not change in the cases of pH 7.0 and 8.0, while a decrease was observed in the cases of pH 8.5 and 9.0. The thermally induced microgel shrinkage may exert two effects on the GNRs attached on the surface of the microgel particles: an increase in the local refractive index and a reduced distance between the nanorods. Both effects will result in the redshifting of the longitudinal plasmon band, however, the former should result in an increased band intensity, while the latter should result in a decreased intensity.[22] The final results should be a combined result of the two opposite effects. From Fig. 1, one can see that the effect of the latter becomes more pronounced with increasing pH. Previously when the thermo-responsive optical properties of GNR-coated PNIPAM microgels were studied, M. Karg *et al.*[22] found that upon heating the intensity of the longitudinal band increases when the surface coverage is low, while it decreases when the surface coverage is high. This is reasonable since plasmon coupling can only take place when the distance between the nanorods is small enough. Therefore the decreased intensity at a higher pH may suggest that higher effective surface coverage was achieved. This hypothesis is in agreement with the observation that the temperature-induced redshift of the plasmon band is larger for samples prepared at higher pH. As summarized in Table 1, the thermally induced redshift is 8, 13, 17 and 19 nm, for pH 7.0, 8.0, 8.5 and 9.0, respectively.

It is noteworthy that the ratio of GNR to microgel is the same for all the samples in this series. The different effective surface coverage suggests that not all the nanorods are sequestered by the microgel particles. This hypothesis was further confirmed by TEM examination. As shown in Fig. 2, for samples prepared at pH 7.0 and 8.0, most of the nanorods exist in the free state. In contrast, most of the nanorods were loaded onto microgel particles when the samples were prepared at pH 8.5 and 9.0. As mentioned above, GNRs are assembled through electrostatic interactions. Although the microgel particles bear some negative charges originating from the ionic initiator,[1] the charge density is

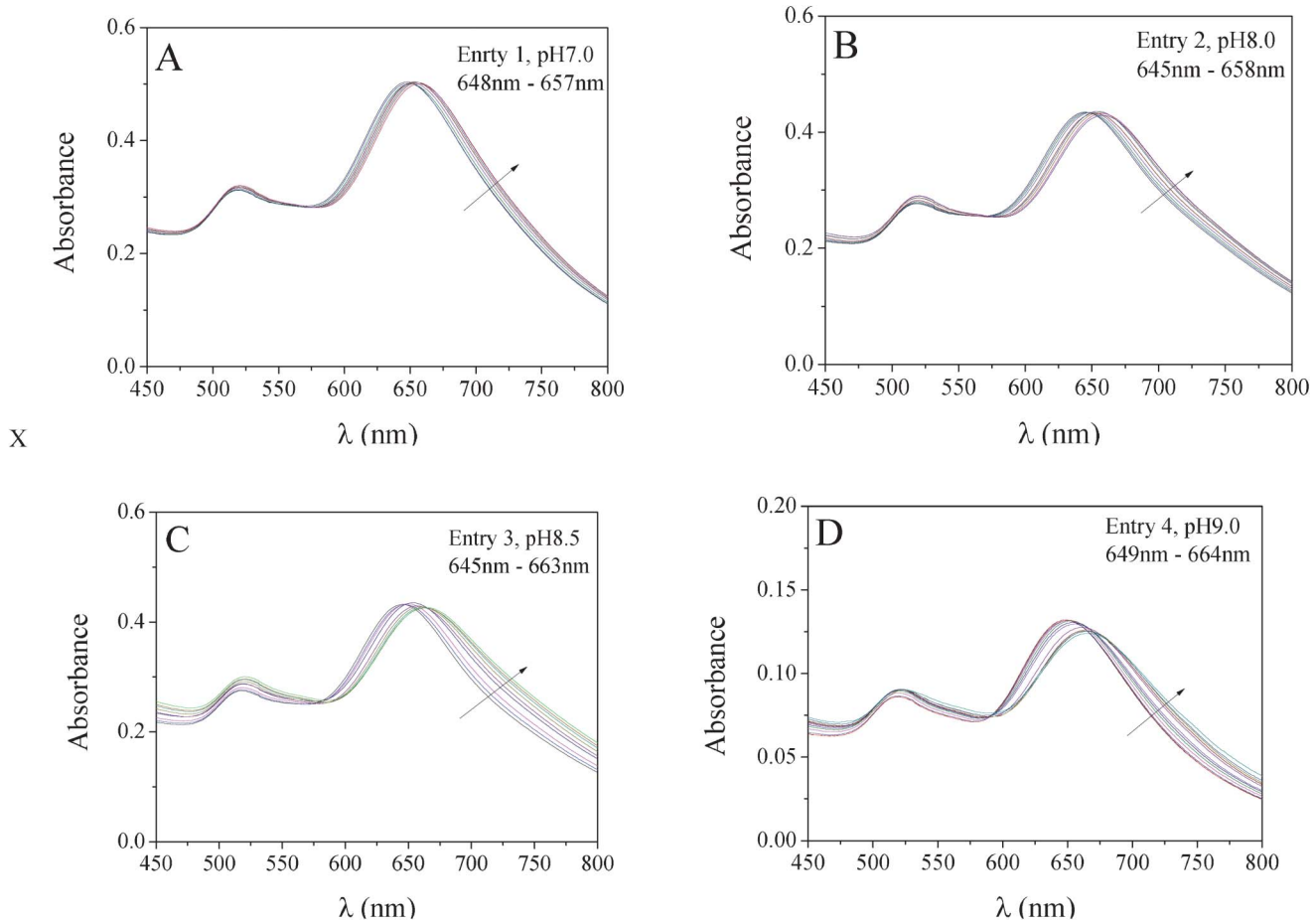

Fig. 1 UV/Vis spectra of the 4 P(NIPAM–AAPBA)/GNR hybrid microgels prepared in Entries 1–4, Table 1. The spectra were measured at different temperatures. (A: 12, 16, 19, 21, 23, 25, 28, 32 °C; B: 12, 14, 16, 18, 20, 22, 24, 26, 30 °C; C: 12, 16, 18, 20, 22, 24, 26, 28, 30 °C; D: 16, 18, 20, 22, 24, 26, 28, 30, 32, 34, 36, 38 °C) Arrows indicate temperature from low to high.

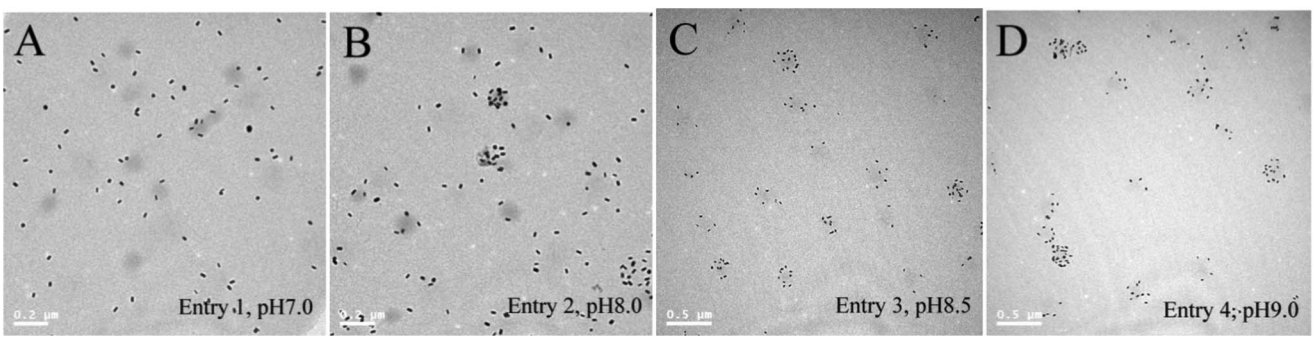

Fig. 2 TEM images of the 4 P(NIPAM–AAPBA)/GNR hybrid microgels prepared in Entries 1–4, Table 1.

not high enough to capture all the nanorods. However, as the pH increases, the PBA groups in the microgels dissociate gradually (pK_a of PBA is ~8.2[47]), thus increasing the surface charge density of the microgel particles. To confirm this, the zeta potentials of the microgel particles were measured to be −3.91, −4.59, −6.89 and −12.13 mV, for particles dispersed in buffers with a pH of 7.0, 8.0, 8.5 and 9.0, respectively. Although in the case of PNIPAM-based microgels, as they are soft colloids, the zeta potential can not be taken as an absolute measure of the surface charge, higher zeta potentials can still reflect the fact that the surface charge density is higher at higher pH.[36] Because of the higher surface charge density at higher pH, GNRs can be sequestered more effectively, resulting in a higher coverage of GNRs and hence a larger redshift of the plasmon band.

In the first series of experiments, the largest redshift of the plasmon band is only 19 nm, which is still very small. Therefore a second series of experiments (Entries 3, 5 and 6 in Table 1) were conducted to study the effect of the ratio of GNR to microgel. In this series of experiments, pH 8.5 was chosen since we have shown that GNRs can be loaded effectively at this pH. Ratios of

GNR to microgel were expressed as the times to that used in Entry 3. Again the assembly was carried out at ~5 °C by using an ice bath. As shown in Table 1, when the ratio of GNR to microgel increases from 1 in Entry 3 to 2.88 in Entry 5, the thermally-induced redshift in the longitudinal plasmon band increases from 17 nm to 34 nm. When the ratio increases further to 21.6 in Entry 6, a dramatic shift of 106 nm was observed. The corresponding spectra are shown in Fig. 3. From these results, one can see that the redshift of the plasmon band increases with increasing ratio of GNR to microgel.

Since the GNRs can be loaded more effectively at pH 9.0, hybrid microgels were also prepared at this pH while using the same large GNR/microgel ratio (Entry 7, Table 1). As expected, the thermally-induced redshift (175 nm) is even larger. To the best of our knowledge, this is the largest redshift observed from hybrid hydrogels containing gold nanoparticles.[22,23,36,48–50] In M. Karg *et al.*'s first report[22] about GNR-coated PNIPAM microgels, the largest thermally induced shift is only 28 nm. Later they achieved a 55 nm shift by increasing the surface coverage.[36] To the best of our knowledge, the largest redshift reported in the literature up to now was reported by Suzuki and Kawaguchi,[23] who observed a 72 nm shift from their hybrid microgels. Compared with these results, the magnitude of the band shift reported here is much larger. For their application as colorimetric sensors, a larger shift of the plasmon band is certainly highly desirable.

Fig. 4 shows the TEM images of the hybrid microgels prepared in Entries 6 (pH 8.5) and 7 (pH 9.0) of Table 1. Compared with the samples prepared using a lower GNR/microgel ratio (Entries 3 and 4 of Table 1, Fig. 2C and 2D), the surface coverage of nanorods is much higher. Therefore the larger redshifts of these samples should be attributed to higher surface coverage of nanorods, which should further be attributed to the larger GNR/microgel ratio used. One may expect that even larger redshift may be achieved by further increasing the GNR/microgel ratio, unfortunately, the system loses its colloidal stability as the microgel particles aggregate and precipitate from the solution.

Fig. 5 shows the plot of the position of the longitudinal band as a function of temperature for the sample prepared in Entry 6,

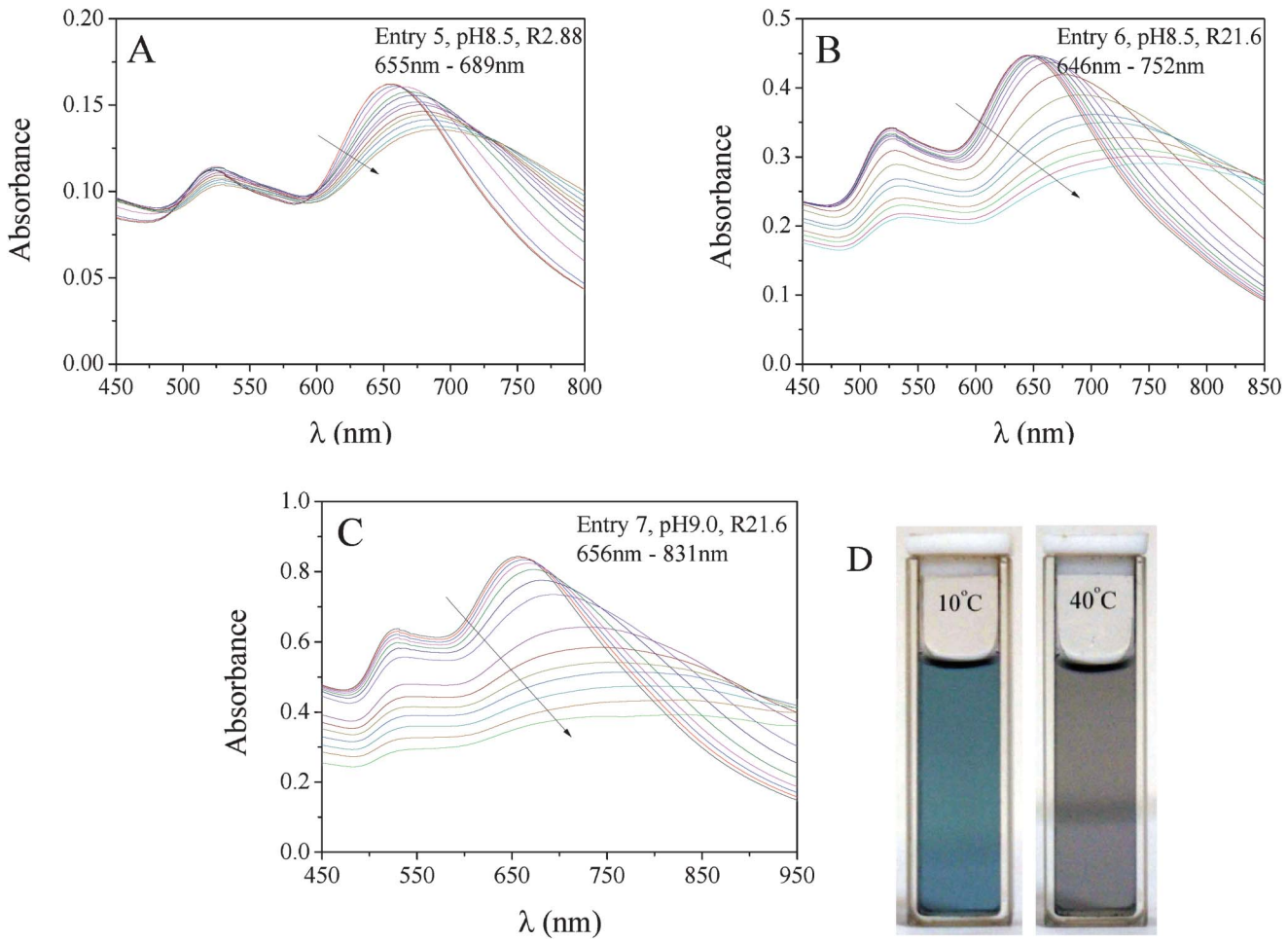

Fig. 3 (A–C) UV/Vis spectra of the 4 P(NIPAM–AAPBA)/GNR hybrid microgels prepared in Entries 5–7, Table 1. The spectra were measured at different temperatures. (A: 16, 18, 20, 22, 24, 26, 28, 30, 32, 34, 36, 38, 40 °C; B: 10, 12, 14, 16, 18, 20, 22, 24, 26, 28, 30, 32, 34, 36, 38, 40 °C; C:14, 16, 18, 20, 22, 24, 26, 28, 30, 32, 34, 36, 38, 40 °C) Arrows indicate temperature from low to high. (D) Photographs of the hybrid microgel at 10 °C (left) and 40 °C (right). The sample was prepared as in Entry 7, Table 1. The samples were all homogenous. The different appearance of the lower part was caused by shadow and background.

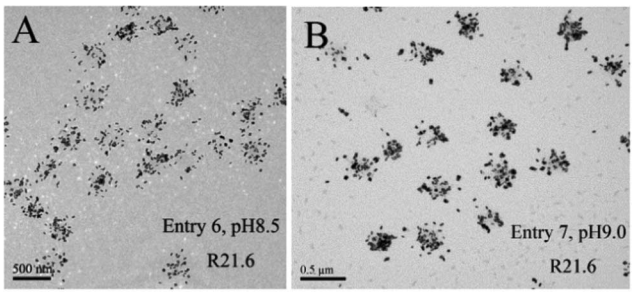

Fig. 4 TEM images of the 2 P(NIPAM–AAPBA)/GNR hybrid microgels prepared in Entries 6 (A) and 7 (B), Table 1.

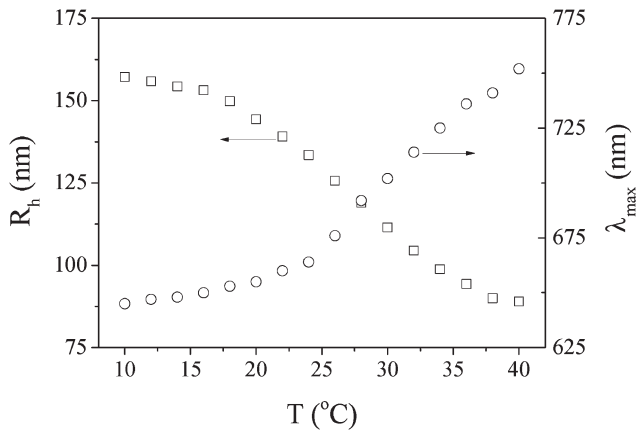

Fig. 5 Maximum of the longitudinal plasmon band (○) and hydrodynamic radii (R_h, □) of the hybrid microgel prepared in Entry 6, Table 1, as a function of temperature.

Table 1. For comparison, the corresponding size of the hybrid microgel was also plotted. The thermally induced shift of the plasmon band corresponds very well with the phase transition of the microgel, confirming the hypothesis that the shrinkage of the microgel particle reduces the distance between the surface-loaded nanorods, thus allowing plasmon coupling to occur and finally resulting in the redshift of the plasmon band.

In accordance with the large shift of the plasmon band in absorption spectra, the color of the sample changes too. As shown in Fig. 3D, at 10 °C the hybrid microgel is blue in color. The sample color changes gradually with increasing temperature. It finally turns to be grey when heated to 40 °C. The color change can be easily detected by the naked eye. Therefore the hybrid microgel can be used to detect temperature either by the shift of plasmon band or directly by color change.

Temperature and glucose sensitive behavior of the hybrid microgels

The thermal phase transition of the hybrid microgel has already been shown in Fig. 5. In Fig. 6, it was compared with the thermal phase transition of the parent P(NIPAM–AAPBA) microgel. Some important information about the structure of the hybrid microgel can be revealed from the comparison. First, the hybrid microgel is larger than the bare microgel in the temperature range we examined. When both microgels are in a fully swollen state, the radius of the hybrid microgel is ~14.0 nm larger than that of the bare microgel. The radius increase when both

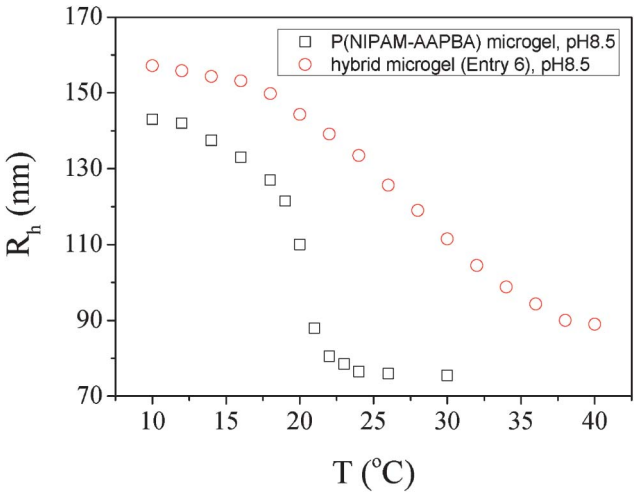

Fig. 6 Hydrodynamic radii (R_h) of the P(NIPAM–AAPBA) microgel and hybrid microgel prepared in Entry 6 , Table 1, as a function of temperature.

microgels are fully collapsed is almost the same (~12.5 nm). The observed radius increase corresponds very well with the diameter of the GNRs (~13.0 nm), suggesting the size increase of the hybrid microgel should be attributed to the addition of a "layer" of GNRs on its surface. Similar to the parent microgel, the hybrid microgel is thermosensitive too, *i.e.*, it shrinks upon heating. Its VPTT (volume phase transition temperature), defined as the onset of the phase transition, is almost the same as that of the parent microgel, suggesting the loading of GNRs does not change the hydrophilic/hydrophobic balance of the microgel. Although the phase transition starts at the same temperature (~18 °C), it ends at a very different temperature. For the parent microgel, it ends at ~22 °C, resulting in a rather sharp transition. In contrast, the hybrid microgel does not collapse completely until the temperature rises to ~38 °C. Similar widened transition have been observed when PNIPAM microgels were highly crosslinked,[51] which is connected with the high heterogeneity brought by the crosslinker.[52] Therefore the widened transition of the hybrid microgel may be explained by an increased effective crosslink density. However, since the GNRs exist mainly on the surface of the microgel particles as revealed above, it is not likely that they will significantly increase the crosslink density of the particles. A more reasonable explanation can be rationalized from the core/shell-like structure of the particle. As mentioned above, the hybrid microgel is actually composed of a thermosensitive P(NIPAM–AAPBA) core and a non-thermosensitive shell of GNRs. When the thermosensitive core collapses upon heating, its deswelling will be retarded by the non-thermosensitive shell, thus resulting in a widened transition. Similar interactions between the core and the shell in core–shell microgels have been reported previously.[51,53–58]

We have previously shown that the P(NIPAM–AAPBA) microgel is glucose-sensitive, *i.e.*, it swells to a larger degree in the presence of glucose.[5,15,16,57] The glucose-sensitivities of the parent microgel and the hybrid microgel were studied at 25 °C in pH 8.5 buffer and 30 °C pH 9.0 buffer. As shown in Fig. 7, a dramatic glucose-induced swelling of the P(NIPAM–AAPBA) microgel was observed under both conditions. For example, in 30 °C pH 9.0 buffer 10 mM glucose increases the hydrodynamic

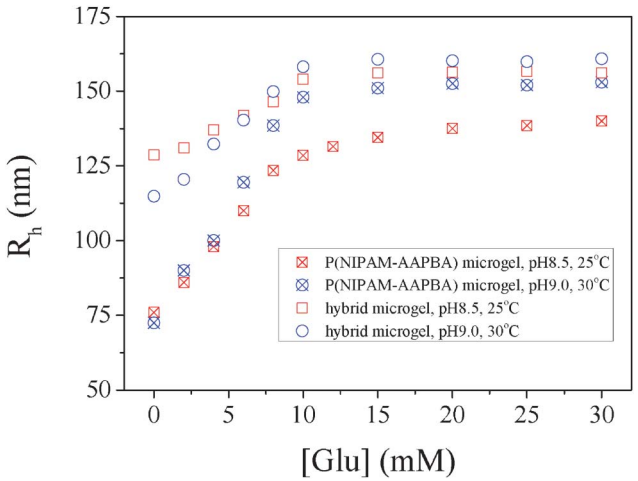

Fig. 7 Hydrodynamic radii (R_h) of the P(NIPAM–AAPBA) microgel and hybrid microgel as a function of glucose concentration.

radius of the microgel from ~73 nm to ~149 nm, corresponding to a 7.5-fold increase in volume. The glucose-induced swelling is attributed to the binding of glucose with PBA groups as shown in Scheme 1. As a result, more PBA groups are converted from the neutral, hydrophobic form to negatively charged, hydrophilic form.[16,59,60] Therefore the microgel swells to a larger degree.

The hybrid microgel remains glucose-sensitive under both conditions studied. The size of microgel first expands with increasing glucose concentration in the solution and flattens off when the glucose concentration is above 10 mM. The trend is similar to that of the bare microgel, however, the extent of the glucose-induced size expansion is reduced. For example, in 30 °C pH 9.0 buffer 10 mM glucose induces a ~76 nm increase in radius for the bare microgel, while it only causes a ~43 nm increase in radius for the hybrid microgel. The reduced size expansion should also be attributed to the restriction of the GNR layer to the swelling of the core.

Colorimetrical detection of glucose

The glucose-induced swelling also affects the optical spectra of the hybrid microgel. As a typical result Fig. 8A shows the absorption spectra of the hybrid microgel measured at 30 °C in pH 9.0 buffer. Before adding glucose, the longitudinal band is located at 724 nm. It gradually shifts to shorter wavelength upon the addition of glucose. At [Glu] = 30 mM, the longitudinal band moves to 673 nm, corresponding to a 51 nm shift. Glucose addition also changes the color of the sample. As shown in

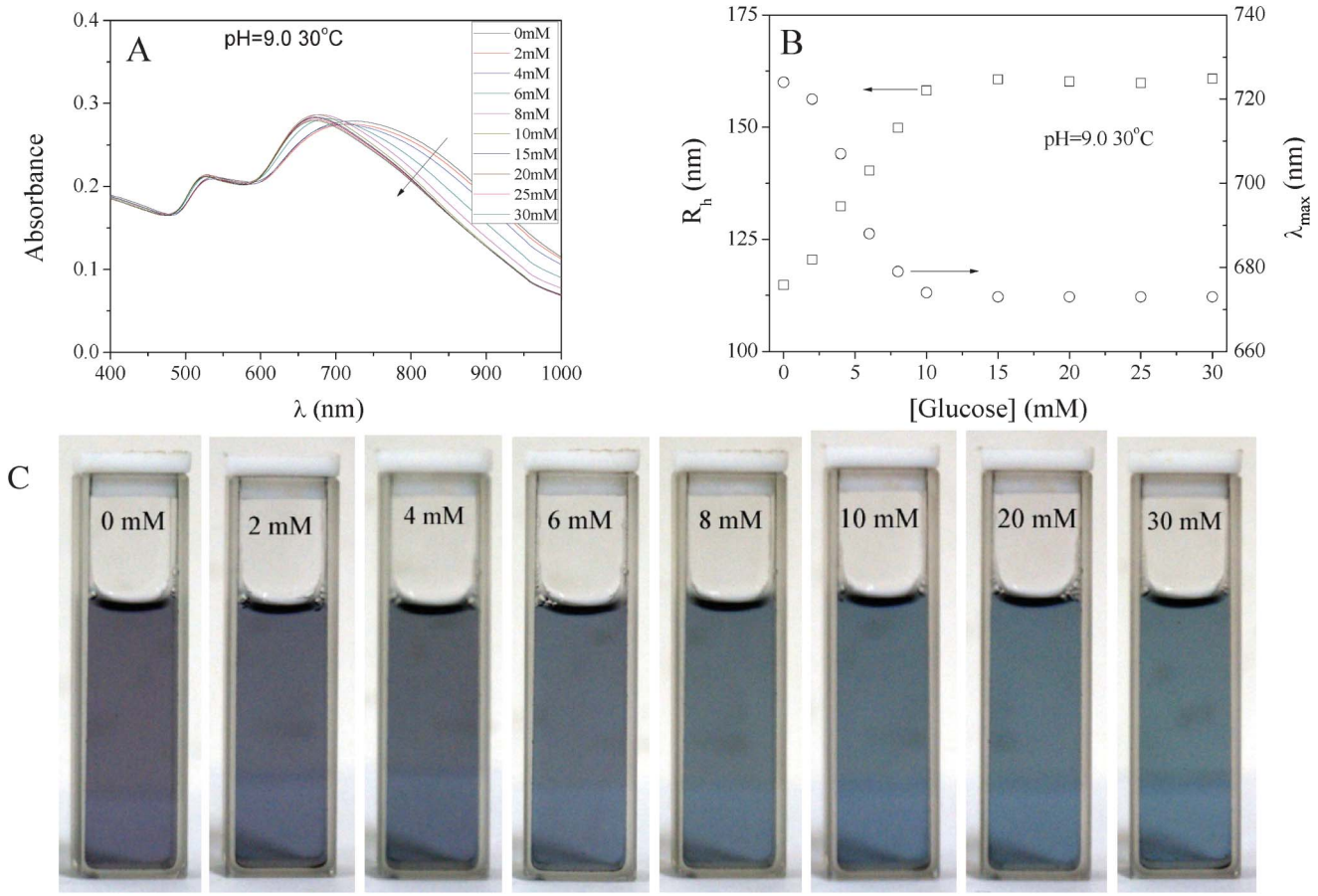

Fig. 8 (A) Evolution of the UV/Vis spectra of the hybrid microgel (prepared in Entry 7, Table 1) upon addition of glucose. pH = 9.0. T = 30 °C. Arrow indicates glucose concentration from low to high. (B) Maximum of the longitudinal plasmon band (○) and hydrodynamic radii (R_h, □) of the hybrid microgel as a function of glucose concentration. (C) Photographs of the hybrid microgel. [Glu] is 0, 2, 4, 6, 8, 10, 20, and 30 mM, from left to right. The samples were all homogenous. The different appearance of the lower part was caused by shadow and background.

Fig. 8C, the dispersion is purple in color in the absence of glucose. It gradually turns to be blue as glucose is added. Therefore glucose can be facilely detected colorimetrically using the hybrid microgel. Glucose-induced blueshift of the plasmon band was also observed from other hybrid microgels prepared in this study.

Fig. 8B plots the position of the longitudinal band as a function of glucose concentration. The corresponding microgel size was plotted for comparison. It is clear that when [Glu] increases from 0 to 10 mM, the microgel swells to a larger degree, thus increasing the distance between the nanorods. As the nanorods separate from each other, the plasmon coupling is reduced, therefore the longitudinal plasmon band shifts to a shorter wavelength. Further increasing [Glu] does not increase the particle size, as a result, the plasmon band stops shifting.

Conclusions

In conclusion the self-assembly of amine modified gold nanorods onto P(NIPAM–AAPBA) microgel particles was studied. We carefully examined the effects of pH and GNR/microgel ratio on the self-assembly. As PBA groups disassociate gradually with increasing pH, the surface charge density of microgel particles increases. Therefore the GNR loading is more effective at higher pH. We also show that the surface coverage of GNR can be effectively increased by using a higher GNR/microgel ratio. Based on these observations, we synthesized hybrid microgels at pH 8.5 and 9.0 using a high GNR/microgel ratio. The very large thermally induced redshift of the longitudinal plasmon band was observed from these hybrid microgels. In agreement with the shift of the plasmon band, the color of the microgel dispersion gradually changes from blue to grey. These hybrid microgels are also glucose-sensitive. Similarly the glucose-induced swelling results in the blueshift of the plasmon band and color change of the dispersion. Therefore using the new hybrid microgel glucose concentration can be facilely detected from the shift of the plasmon band and/or color change.

Acknowledgements

We thank financial support for this work from the Ministry of Science and Technology of China (Grant No. 2007DFA50760) and the National Natural Science Foundation of China (Grant No. 20974049, 20974050 and 2117407).

References

1 B. R. Saunders and B. Vincent, *Adv. Colloid Interface Sci.*, 1999, **80**, 1–25.
2 R. Pelton, *Adv. Colloid Interface Sci.*, 2000, **85**, 1–33.
3 Y. Guan and Y. Zhang, *Soft Matter*, 2011, **7**, 6375–6384.
4 G. R. Hendrickson, M. H. Smith, A. B. South and L. A. Lyon, *Adv. Funct. Mater.*, 2010, **20**, 1697–1712.
5 P. X. Liu, Q. F. Luo, Y. Guan and Y. J. Zhang, *Polymer*, 2010, **51**, 2668–2675.
6 C. M. Nolan, M. J. Serpe and L. A. Lyon, *Biomacromolecules*, 2004, **5**, 1940–1946.
7 Y. Liu, Y. J. Zhang and Y. Guan, *Chem. Commun.*, 2009, 1867–1869.
8 W. T. Wu, T. Zhou, J. Shen and S. Q. Zhou, *Chem. Commun.*, 2009, 4390–4392.
9 J. S. Kim, N. Singh and L. A. Lyon, *Angew. Chem., Int. Ed.*, 2006, **45**, 1446–1449.
10 D. Wang, D. Cheng, Y. Guan and Y. Zhang, *Biomacromolecules*, 2011, **12**, 578–584.
11 T. Gan, Y. Zhang and Y. Guan, *Biomacromolecules*, 2009, **10**, 1410–1415.
12 A. Garcia, M. Marquez, T. Cai, R. Rosario, Z. B. Hu, D. Gust, M. Hayes, S. A. Vail and C. D. Park, *Langmuir*, 2007, **23**, 224–229.
13 T. Hoare and R. Pelton, *Macromolecules*, 2004, **37**, 2544–2550.
14 S. Nayak and L. A. Lyon, *Chem. Mater.*, 2004, **16**, 2623–2627.
15 S. Xing, Y. Guan and Y. Zhang, *Macromolecules*, 2011, **44**, 4479–4486.
16 Y. J. Zhang, Y. Guan and S. Q. Zhou, *Biomacromolecules*, 2006, **7**, 3196–3201.
17 V. Lapeyre, I. Gosse, S. Chevreux and V. Ravaine, *Biomacromolecules*, 2006, **7**, 3356–3363.
18 T. Hoare and R. Pelton, *Macromolecules*, 2007, **40**, 670–678.
19 Q. Luo, Y. Guan, Y. Zhang and M. Siddiq, *J. Polym. Sci., Part A: Polym. Chem.*, 2010, **48**, 4120–4127.
20 X. J. Ju, L. Liu, R. Xie, C. H. Niu and L. Y. Chu, *Polymer*, 2009, **50**, 922–929.
21 M. Karg and T. Hellweg, *Curr. Opin. Colloid Interface Sci.*, 2009, **14**, 438–450.
22 M. Karg, I. Pastoriza-Santos, J. Perez-Juste, T. Hellweg and L. M. Liz-Marzan, *Small*, 2007, **3**, 1222–1229.
23 D. Suzuki and H. Kawaguchi, *Langmuir*, 2006, **22**, 3818–3822.
24 W. T. Wu, N. Mitra, E. Yan and S. Q. Zhou, *ACS Nano*, 2010, **4**, 4831–4839.
25 B. Brugger and W. Richtering, *Adv. Mater.*, 2007, **19**, 2973–2978.
26 R. Contreras-Caceres, S. Abalde-Cela, P. Guardia-Giros, A. Fernandez-Barbero, J. Perez-Juste, R. A. Alvarez-Puebla and L. M. Liz-Marzan, *Langmuir*, 2011, **27**, 4520–4525.
27 S. Carregal-Romero, N. J. Buurma, J. Perez-Juste, L. M. Liz-Marzan and P. Herves, *Chem. Mater.*, 2010, **22**, 3051–3059.
28 Y. Lu, Y. Mei, M. Drechsler and M. Ballauff, *Angew. Chem., Int. Ed.*, 2006, **45**, 813–816.
29 P. K. Jain, X. H. Huang, I. H. El-Sayed and M. A. El-Sayed, *Acc. Chem. Res.*, 2008, **41**, 1578–1586.
30 N. Nath and A. Chilkoti, *J. Fluoresc.*, 2004, **14**, 377–389.
31 J. Pérez-Juste, I. Pastoriza-Santos, L. M. Liz-Marzán and P. Mulvaney, *Coord. Chem. Rev.*, 2005, **249**, 1870–1901.
32 J. Stone, S. Jackson and D. Wright, *Wiley Interdiscip. Rev.: Nanomed. Nanobiotechnol.*, 2011, **3**, 100–109.
33 C. Yu and J. Irudayaraj, *Anal. Chem.*, 2006, **79**, 572–579.
34 I. S. Lim, D. Mott, W. Ip, P. N. Njoki, Y. Pan, S. Zhou and C. Zhong, *Langmuir*, 2008, **24**, 8857–8863.
35 P. K. Sudeep, S. T. S. Joseph and K. G. Thomas, *J. Am. Chem. Soc.*, 2005, **127**, 6516–6517.
36 M. Karg, Y. Lu, E. Carbo-Argibay, I. Pastoriza-Santos, J. Perez-Juste, L. M. Liz-Marzan and T. Hellweg, *Langmuir*, 2009, **25**, 3163–3167.
37 M. Das, N. Sanson, D. Fava and E. Kumacheva, *Langmuir*, 2007, **23**, 196–201.
38 M. Das, L. Mordoukhovski and E. Kumacheva, *Adv. Mater.*, 2008, **20**, 2371–2375.
39 Y. Lu, J. Yuan, F. Polzer, M. Drechsler and J. Preussner, *ACS Nano*, 2010, **4**, 7078–7086.
40 M. Karg, S. Jaber, T. Hellweg and P. Mulvaney, *Langmuir*, 2011, **27**, 820–827.
41 R. Contreras-Caceres, J. Pacifico, I. Pastoriza-Santos, J. Perez-Juste, A. Fernandez-Barbero and L. M. Liz-Marzan, *Adv. Funct. Mater.*, 2009, **19**, 3070–3076.
42 N. Singh and L. A. Lyon, *Chem. Mater.*, 2007, **19**, 719–726.
43 X. Liu, F. Cheng, Y. Liu, W. Li, Y. Chen, H. Pan and H. Liu, *J. Mater. Chem.*, 2010, **20**, 278–284.
44 N. R. Jana, *Small*, 2005, **1**, 875–882.
45 C. Wang and J. Irudayaraj, *Small*, 2008, **4**, 2204–2208.
46 I. Gorelikov, L. M. Field and E. Kumacheva, *J. Am. Chem. Soc.*, 2004, **126**, 15938–15939.
47 A. Matsumoto, R. Yoshida and K. Kataoka, *Biomacromolecules*, 2004, **5**, 1038–1045.
48 D. Suzuki and H. Kawaguchi, *Langmuir*, 2005, **21**, 8175–8179.
49 V. Kozlovskaya, E. Kharlampieva, B. P. Khanal, P. Manna, E. R. Zubarev and V. V. Tsukruk, *Chem. Mater.*, 2008, **20**, 7474–7485.
50 K. Akamatsu, M. Shimada, T. Tsuruoka, H. Nawafune, S. Fujii and Y. Nakamura, *Langmuir*, 2010, **26**, 1254–1259.
51 C. D. Jones and L. A. Lyon, *Macromolecules*, 2003, **36**, 1988–1993.

52 C. Wu and S. Zhou, *Macromolecules*, 1997, **30**, 574–576.
53 I. Berndt, J. S. Pedersen and W. Richtering, *J. Am. Chem. Soc.*, 2005, **127**, 9372–9373.
54 C. Chi, T. Cai and Z. Hu, *Langmuir*, 2009, **25**, 3814–3819.
55 S. Schachschal, A. Balaceanu, C. Melian, D. E. Demco, T. Eckert, W. Richtering and A. Pich, *Macromolecules*, 2010, **43**, 4331–4339.
56 T. Hellweg, C. D. Dewhurst, W. Eimer and K. Kratz, *Langmuir*, 2004, **20**, 4330–4335.
57 Q. F. Luo, P. X. Liu, Y. Guan and Y. J. Zhang, *ACS Appl. Mater. Interfaces*, 2010, **2**, 760–767.
58 Y. J. Zhang, Y. Guan and S. Q. Zhou, *Biomacromolecules*, 2007, **8**, 3842–3847.
59 S. A. Asher, V. L. Alexeev, A. V. Goponenko, A. C. Sharma, I. K. Lednev, C. S. Wilcox and D. N. Finegold, *J. Am. Chem. Soc.*, 2003, **125**, 3322–3329.
60 K. Kataoka, H. Miyazaki, M. Bunya, T. Okano and Y. Sakurai, *J. Am. Chem. Soc.*, 1998, **120**, 12694–12695.